THE EUROPEAN
PHYSICAL JOURNAL D

Regular Article

Radiative cooling of carbon cluster anions C_{2n+1}^- (n = 3−5)[⋆]

Mark H. Stockett[1,a], James N. Bull[2], Jack T. Buntine[3], Eduardo Carrascosa[4], Emma K. Anderson[1],
Michael Gatchell[1,5], Magdalena Kaminska[1], Rodrigo F. Nascimento[1,6], Henrik Cederquist[1], Henning T. Schmidt[1],
and Henning Zettergren[1]

[1] Department of Physics, Stockholm University, Stockholm, Sweden
[2] School of Chemistry, University of East Anglia, Norwich, UK
[3] School of Chemistry, University of Melbourne, Melbourne, Australia
[4] Laboratoire de Chimie Physique Moléculaire, Ecole Polytechnique Fédérale de Lausanne, EPFL SB ISIC LCPM, Station 6,
CH-1015 Lausanne, Switzerland
[5] Institute for Ion Physics and Applied Physics, University of Innsbruck, Innsbruck, Austria
[6] Centro Federal de Educação Tecnológica Celso Suckow da Fonseca, Petrópolis, Brazil

Abstract. Radiative cooling of carbon cluster anions C_{2n+1}^- (n = 3−5) is investigated using the cryogenic electrostatic ion storage ring DESIREE. Two different strategies are applied to infer infrared emission on slow (milliseconds to seconds) and ultraslow (seconds to minutes) timescales. Initial cooling of the ions over the millisecond timescale is probed indirectly by monitoring the decay in the yield of spontaneous neutralization by thermionic emission. The observed cooling rates are consistent with a statistical model of thermionic electron emission in competition with infrared photon emission due to vibrational de-excitation. Slower cooling over the seconds to minutes timescale associated with infrared emission from low-frequency vibrational modes is probed using time-dependent action spectroscopy. For C_9^- and C_{11}^-, cooling is evidenced by the time-evolution of the yield of photo-induced neutralization following resonant excitation of electronic transitions near the detachment threshold. The cross-section for resonant photo-excitation is at least two orders of magnitude greater than for direct photodetachment. In contrast, C_7^- lacks electronic transitions near the detachment threshold.

1 Introduction

One of the hallmarks of the physics of atomic clusters is the dramatic variation of their properties and stability with size [1]. For both static properties such as electron affinity and dynamic properties such as radiative cooling rates, every atom matters [2,3]. However, radiative cooling rates, particularly those occurring on slow (e.g. milliseconds to seconds) and ultraslow (e.g. longer than seconds) timescales, are difficult to measure due to challenges associated with storing ions in a collision free environment for extended periods of time. Notwithstanding, radiative cooling rates are thought to be a crucial factor in the formation and stabilization of carbonaceous ions in space [4,5]. While static properties of carbon cluster anions, such as electron affinities, have been well-studied following the identification of species like $C_{2n}H^-$ (n = 2−4) [6–8] and $C_{2n+1}N^-$ (n = 0−2) [9–11] in interstellar molecular clouds, there is

limited data on radiative cooling rates and competitions between cooling and anion destruction mechanisms.

Since the turn of the century, radiative cooling rates of clusters have been inferred from experiments probing time-dependent spontaneous neutralization rates of ensembles of hot ions stored in electrostatic ion-beam storage devices (see e.g. [12–21]). Such devices have been used to isolate and probe the cooling of cluster ions for durations of up to tens of milliseconds. The radiative cooling in this time regime is usually dominated by one or two strongly infrared active modes [20], or by recurrent fluorescence [22,23] i.e. emission due to decay of thermally populated electronically excited states. The advent of a new generation of cryogenically cooled electrostatic storage devices has extended the time range for observations of spontaneous neutralization to several seconds [24–27].

In a recent study we developed a strategy for probing ultraslow radiative cooling of carbon cluster anions, C_n^- (n = 3−5) [28]. The strategy involves construction of two-dimensional (i.e. storage time dependent) near-threshold photodetachment action spectra. Rates associated with infrared cooling can be ascertained by monitoring the disappearance of hot-band signal with ion storage
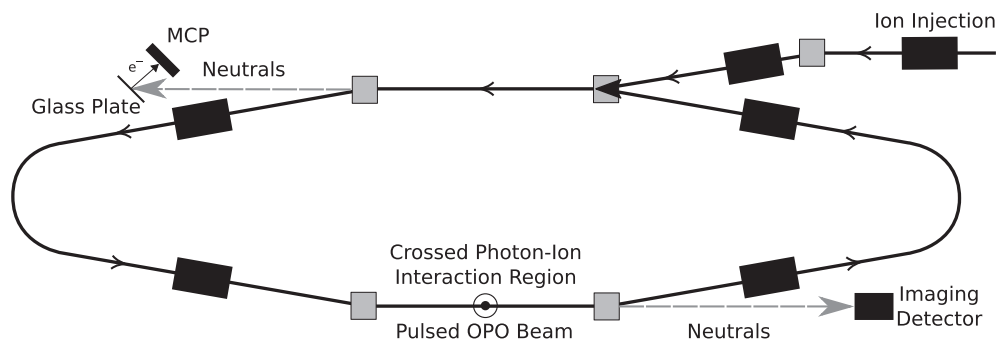

Fig. 1. The symmetric ion storage ring in DESIREE [30,31]. Neutral particles formed following laser excitation in the lower straight region (crossed-beam geometry with the optical parametric oscillator, OPO) are detected in the forward direction with the Imaging Detector. Neutrals produced through thermionic emission in either straight section strike the Imaging Detector or the Glass Plate/MCP detector.

time. This strategy allows investigation of cooling associated with infrared modes of lower frequency and modes with lower decay rates; it is not possible to study these dynamics in room-temperature ion storage rings. As part of this study, we developed a simple harmonic cascade (SHC) model of infrared radiative cooling, which satisfactorily described the experimental data. A similar two-dimensional action spectroscopy strategy to probe cooling dynamics, although using Multi-Photon Dissociation, has been applied to probe the radiative cooling of Polycyclic Aromatic Hydrocarbon cations [29].

Here, we extend our earlier study on C_n^- ($n = 3-5$) to larger cluster anions C_{2n+1}^- ($n = 3-5$). We first examined the spontaneous neutralization of these anions on the sub-second timescale, where radiative cooling competes with thermionic emission of electrons. Secondly, we applied the 2D near-threshold photodetachment action spectroscopy strategy to monitor cooling over the slower (seconds to minutes) timescale where only radiative cooling through infrared photon emission is important. Both sets of results are interpreted within the framework of the SHC radiative cooling model.

2 Methods

2.1 Experiments

Experiments were performed at the DESIREE (Double ElectroStatic Ion Ring ExpEriment) storage ring facility located at the Department of Physics, Stockholm University [30,31]. The symmetric storage ring used in this study is schematically illustrated in Figure 1. The vacuum chamber, electrostatic deflectors and detectors are cooled to ≈ 13 K by helium refrigerators, providing ultra-high vacuum conditions that allow storage of keV ion beams for hours [32,33]. The target anions, C_{2n+1}^- ($n = 3-5$), were produced using a caesium sputtering ion source (National Electrostatics Corp., Madison, Wisconsin) with a graphite cathode. The sputtering process generates ions with high degrees of rovibrational excitation, i.e. source-heated ions [14,19]. The nascent ions were accelerated to 10 keV (8 keV for C_7^- action spectroscopy measurements),

selected according to their mass-to-charge ratio using a bending magnet, and injected into the storage ring [30]. Transport from the source to the ring takes $\approx 80-100\,\mu$s and the $1/e$ beam storage lifetimes are typically >100 s, limited by loss of ions through collisions with background gas of $\sim 10^4$ H$_2$ molecules per cm^3 [28,31].

The ions initially stored in the ring have a broad distribution of internal excitations, similar to thermal distributions with temperatures exceeding 1000 K [26]. Ions with internal energies exceeding the adiabatic detachment energy may spontaneously neutralize via thermionic emission. Dissociation of the ions is also possible in principle, however, in the present case the dissociation energies are sufficiently high such that dissociation processes will not be observed within the experimental time window. Such hot ions will decay at higher rates and would thus not survive the transport to the storage ring. Neutrals formed in one of the two straight sections of the storage ring are unaffected by the electrostatic steering fields and impact on one of the two particle detectors consisting of micro-channel plates (MCPs) ("MCP" and "Imaging Detector" in Fig. 1) [34,35].

For the action spectroscopy experiments, which probe cooling on the ultraslow timescale, stored ions were irradiated with tunable-wavelength light from an optical parametric oscillator (OPO, EKSPLA NT342B, 10 Hz) using a crossed-beam geometry in one of the straight sections of the ion storage ring ("Interaction Region" in Fig. 1). Any neutral particles formed through photodetachment or photodissociation in the first few microseconds after irradiation will strike the Imaging Detector (see Fig. 1) [34]. The signal from this MCP detector was gated using a 1 μs gate pulse which was slightly delayed with respect to the OPO pulse to account for the neutral particles' flight time to the detector. The purpose of the gate was to eliminate signal from scattered OPO light striking the detector and to minimize background counts. Stored ions were irradiated repeatedly every 100 ms at a given OPO wavelength for a pre-set ion storage time (3–90 s). The irradiation wavelength was stepped in 0.5 nm increments (≈ 0.005 eV photon energy) between ion injections, providing a time dependent photo-action yield at each wavelength, or alternatively a series of action spectra at different storage times. The full dataset is referred to as the 2D action
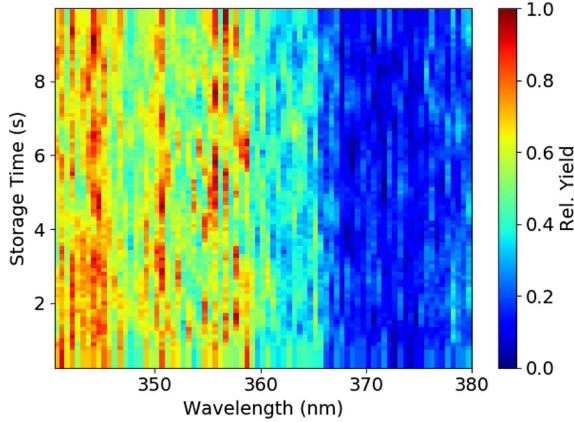
Fig. 2. Two-dimensional (2D) action spectrum of C_7^-.

spectrum. As an example, the 2D action spectrum of C_7^- is presented in Figure 2. The wavelength accuracy of the OPO is better than 0.05 nm, as measured with an optical spectrograph. The OPO light pulse energy was less than 2 mJ.

2.2 Modeling

Infrared radiative cooling was modelled using a SHC model [28]. Briefly, the model utilizes the vibrational density of states ρ computed with the Beyer–Swinehart algorithm and scaled harmonic vibrational mode frequencies ν_s calculated at the ωB97X-D//aug-cc-pVTZ level of Density Functional Theory (DFT) in Gaussian 16 [36–38]. The calculated vibrational frequencies are tabulated in Appendix A. For a vibrational level with energy E, the infrared radiative cooling rate coefficient k_s for a given mode s is [23]

$$k_s(E) = A_s^{10} \sum_{v=1}^{v \le E/h\nu_s} \frac{\rho(E - vh\nu_s)}{\rho(E)}, \qquad (1)$$

where h is Plank's constant. In the Simple Harmonic Cascade (SHC) model, only transitions that involve the vibrational quantum number v decreasing by one quanta are considered, i.e. $\Delta v = -1$. The Einstein coefficients A_s^{10} for $v = 1 \rightarrow v = 0$ transitions were taken from our DFT calculations (see Appendix A). The total cooling rate is given by $k_{tot} = \sum_s k_s$. Recurrent fluorescence, which has been observed for carbon cluster anions with even numbers of atoms [23,39,40], is not expected to play a significant role in the cooling dynamics of the present target ions. Anions with odd numbers of carbon atoms lack the low-lying electronic states which are required for recurrent fluorescence to compete with thermionic emission [41].

The rate coefficient for thermionic emission is approximately given by [42]

$$k_e(E) = \omega \frac{\rho_0(E - \Phi)}{\rho(E)}, \qquad (2)$$

where ρ_0 is the density of states of the neutral cluster and Φ is the adiabatic detachment energy, taken from

photoelectron spectroscopy measurements [43,44]. The pre-exponential factor ω is proportional to the electron capture cross section [42] and is here approximated as a constant equal to $10^{14}\,\mathrm{s}^{-1}$ [20]. In the simulations, we found that the value of ω could be varied by more than 6 orders of magnitude without changing the shape of the spontaneous decay curves.

Starting from an initial Boltzmann distribution of vibrational energy $g(E, t = 0)$ normalized such that $\int g(E, t = 0)dE = 1$, the population distribution $g(E, t)$ was propagated in $50\,\mu$s timesteps using the master equation approach [45]. The initial Boltzmann temperature did not substantially alter the shape of the spontaneous decay curves, provided that the high-energy tail of the distribution extended well above Φ. The neutral yield is $\Gamma(t) = \int k_e(E)g(E, t)dE$.

For ion storage times longer than 100 ms, where the spontaneous neutralization yield becomes negligibly low, the total energy remaining in the ensemble as a function of time, $E_{tot}(t) = \int Eg(E, t)dE$, was taken as an indicator of the cooling of the ensemble. The simulation timestep was allowed to grow dynamically in proportion to the decay time of the highest energy level with significant remaining population.

For small carbon cluster anions, the dominant unimolecular dissociation channel observed experimentally is the loss of neutral C_3, i.e. $C_n^- \rightarrow C_{n-3}^- + C_3$ [46,47]. For C_7^-, C_9^-, and C_{11}^-, calculated dissociation energies are 5.77 eV, 5.53 eV, and 5.41 eV, respectively [48]. Ions with internal energies exceeding the dissociation energy could fragment over the 80–100 μs flight time required for transport from the ion source to the storage ring. Dissociation is thus not included in our modelling.

3 Results and discussion

3.1 Spontaneous decay

The neutralization rates for beams of source heated C_{2n+1}^- ($n = 3-5$) ions, measured using the Glass Plate/MCP detector in Figure 1, are shown in Figure 3. For C_7^-, the result agrees well with a previous room-temperature investigation by Najafian et al. [20]. The nearly constant neutralization signal for storage times longer than $\approx$5 ms is due to collisions between the stored ions and residual gas [31]. The detector dark count rate was measured at $\approx$20% of the residual gas background signal by recording signal over a 5 ms window prior to injection of the ion beam. Dark counts have been subtracted from the data plotted in Figure 3. This collision-induced neutralization at times longer than $\approx$5 ms shows that a large number of ions remain stored after the disappearance of the initial signal [31]. The higher neutralization rate at early times is attributed to spontaneous neutralization (thermionic emission) of the small fraction of ions with internal energies that exceed the detachment threshold Φ.

Source-heated ions with internal energy exceeding Φ can undergo two distinct processes: (i) neutralization by thermionic emission, and (ii) cooling by infrared photon
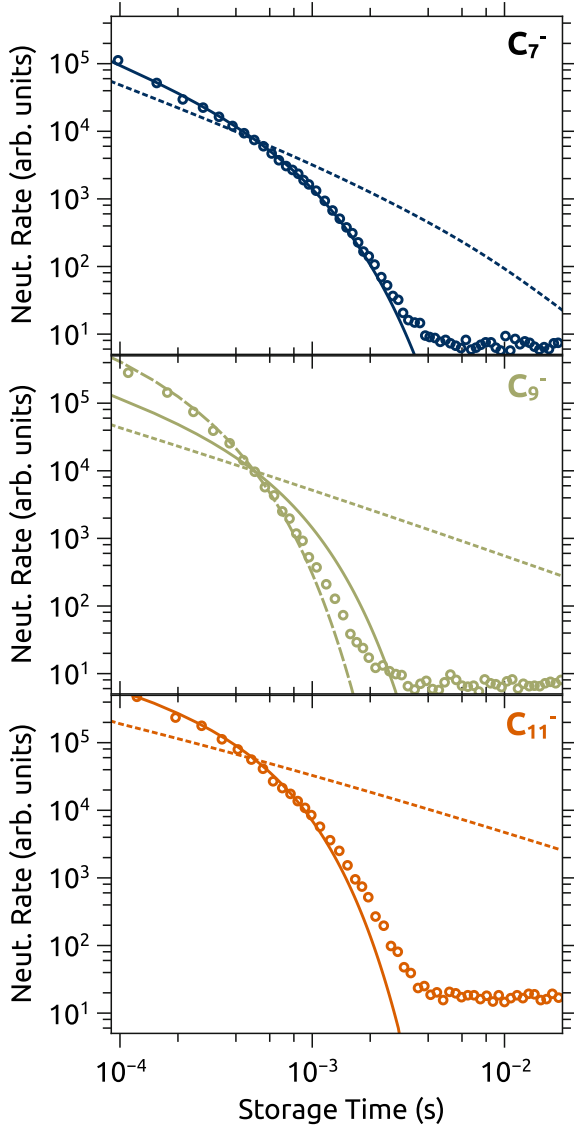
Fig. 3. Neutralization of stored ion beams of C_{2n+1}^- ($n = 3-5$). Open circles: experimental data; dotted lines: simulation without radiative cooling; solid lines: simulation with radiative cooling; dashed line (C_9^- only): simulation with cooling rate multiplied by a factor of two to achieve best agreement with experiment.

Table 1. Fit parameters P and τ for spontaneous neutralization yield, values of $\tau \approx k_{tot}(\Phi)^{-1}$ from our SHC model, and adiabatic detachment energies (Φ) from literature [43,44]. Statistical uncertainties in the last digit are given in parentheses.

	P	τ (ms)	$k_{tot}(\Phi)^{-1}$ (ms)	Φ (eV)
C_7^-	1.36 (2)	0.75 (3)	0.59	3.3517 (4)
C_9^-	0.82 (4)	0.182 (5)	0.37	3.6766 (14)
C_{11}^-	0.92 (3)	0.41 (2)	0.26	3.913 (8)

energies below Φ are stable and continue to orbit in the storage ring with a storage lifetime of hundreds of seconds, limited by collisions with residual gas.

The thermionic emission rate coefficient $k_e(E)$ depends upon the internal energy and increases rapidly across the energy window $\Phi < E < \Phi + 0.5$ eV. For an ensemble of ions, the corresponding neutralization rate Γ decreases with time according to a power law $\Gamma \propto t^{-P}$ ($P \approx 1$) [25,49]. Radiative cooling "quenches" this power-law decay [12,13] after a characteristic critical time, τ, which can be approximated as the inverse of the radiative cooling rate constant at an energy equal to Φ, i.e. $\tau \approx 1/k_{tot}(\Phi)$. Fits to the quenched power law $\Gamma \propto t^{-P}e^{-t/\tau}$ yielded the parameters given in Table 1, with τ ranging from a few tenths of a millisecond (C_9^-) to near one millisecond (C_7^-).

Results of our simulations without radiative cooling (dotted line) and with radiative cooling according to the SHC model (solid line) are included in Figure 3. Simulations incorporating radiative cooling agree well with the experimental data for C_7^- and C_{11}^-. For C_9^-, the radiative cooling rate k_{tot} has to be adjusted by a factor of two to achieve best agreement with experiment. Considering the approximations of the SHC model, such as the neglect of most anharmonic effects, the agreement between theory and experiment is most satisfactory.

3.2 Action spectroscopy

Action spectra for C_{2n+1}^- ($n = 3-5$) are shown in Figure 4. For C_9^- and C_{11}^-, this spectrum was constructed by integrating the 2D action spectra (not shown) over 3 s of storage time, with the integration excluding the first laser shot just after injection when the thermionic emission rate is still significant. For the C_7^- spectrum, the spectrum was constructed using by integrating a storage time of 10 s for each photon energy (wavelength). In each panel in Figure 4, the adiabatic detachment energy (Φ) determined from photo-electron spectroscopy [43,44] is indicated by a vertical dashed line. For C_9^- and C_{11}^-, the vertical bars indicate the energies of electronically excited states of the anion, measured by Forney et al. in a neon matrix [50].

The action spectrum of C_7^- is attributed predominantly to direct photodetachment, and shows a clear Wigner-type threshold behavior above the adiabatic detachment energy [51], similar to the results of Bull et al. for C_n^- ($n = 3-5$) [28]. However, unlike in the study of Bull et al. [28], no

emission. Thermionic emission removes population from the high-energy part of the distribution and gives rise to the neutral clusters detected in the experiment, while infrared cooling (which does not yield neutrals) may lower the vibrational energy from a level above Φ to a level below Φ; the ion will be unable to eject an electron thereafter. Our simulations predict that the neutralization signal originating from spontaneous (thermionic) electron emission is due to ions with internal energies in a narrow band of $0-0.5$ eV above Φ. The simulations suggest that ions with significantly higher internal energies (including those with enough energy to dissociate) decayed during the initial $\approx 80-100$ μs interval when they were transported from the ion source to the storage ring. Ions with
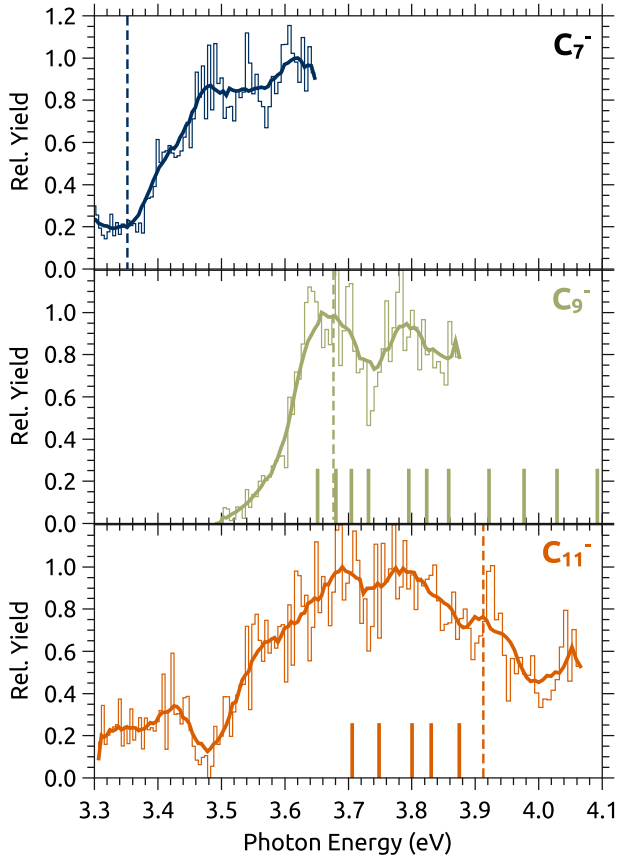
Fig. 4. Storage time-integrated action spectra for C_{2n+1}^- ($n = 3-5$). The heavy solid lines are 10-point moving averages. Vertical dashed lines show the adiabatic detachment energies reported from photo-electron spectroscopy [43,44]. Vertical bars show energies of electronic transitions of C_9^- and C_{11}^- from matrix isolation spectroscopy [50].
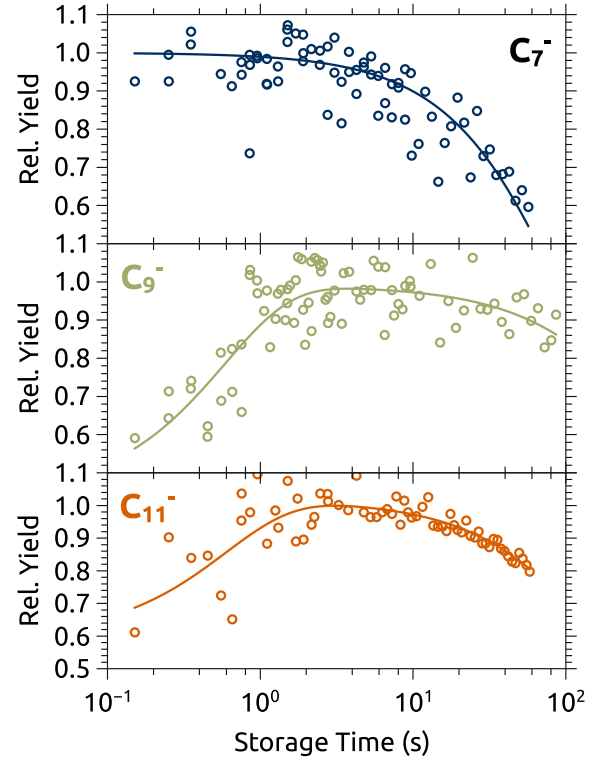

Fig. 5. Total photo-action yields for C_{2n+1}^- ($n = 3-5$) with ion storage time. The solid line is a fit with exponential growth and decay components.

significant time-dependent contribution due to depletion of hot-bands was observed for C_7^- (see Fig. 2 and compare with Fig. 2 in Ref. [28]).

For C_9^- and C_{11}^-, no obvious threshold behaviour is found above the detachment energy. Instead, the action spectra appear to be dominated by resonant excitation to electronically excited states of the anions. The energies of these transitions, measured in a neon matrix [50], are indicated with vertical bars in Figure 4. No such transitions are reported for C_7^- between 3.3 eV and 4.4 eV [50]. For similar ion beam current and laser pulse energy, the photo-action yield was more than two orders of magnitude greater for C_9^- and C_{11}^- compared to C_7^-, further evidencing the role of resonant transitions. It follows that electronic excitation of near-threshold states for C_9^- and C_{11}^- is promptly followed by internal conversion to a vibrationally excited ground electronic state and then thermionic emission to yield neutral particles. In this case, dissociation (perhaps in competition with recurrent fluorescence) may also be possible if the internal energy of the ions *prior to* excitation is sufficiently high that the energy *after* excitation and internal conversion is greater than the dissociation energy. Experimentally, no delayed neutralization

was observed following additional turns around the storage ring.

The storage time dependence of the photo-action yield for C_7^-, C_9^-, and C_{11}^- is shown in Figure 5. This was obtained by integrating 2D spectra across the measured spectral range plotted in Figure 4 (e.g. 3.3–3.55 eV for C_7^-). The solid lines are empirical fits as a guide and to extract characteristic time constants. The fits include exponential growth and decay components, i.e.

$$\Gamma = a_1(1 - e^{-t/\tau_1}) + a_2 e^{-t/\tau_2} \qquad (3)$$

where a_1 and a_2 are constants and τ_1 and τ_2 are characteristic times. Note that equation (3) does not represent any physical model of cooling or relaxation processes, rather it is an empirical expression to describe the trend in the experimental data. For C_7^-, a single exponential decay was fit ($a_1 = 0$) with a time constant $\tau_2 \approx 100$ s. For C_9^- and C_{11}^-, the photo-action signal increases at short storage times (e.g. less than a second) with time constant $\tau_1 \approx 0.5$ s. It is likely that this increase in the photo-action signal is due to recovery of the ground and low-lying vibrational states of the anion, which in turn increases the probability for resonant excitation. A similar effect was previously characterised for C_5^- [28]. The decay in photo-action signal at longer times ($\tau_2 > 100$ s) in Figure 5 is probably associated with the ion beam storage lifetime (≈ 300 s for C_{11}^-), but may have some contribution from further cooling of photo-activated ions that have insufficient vibrational energy to produce neutrals.
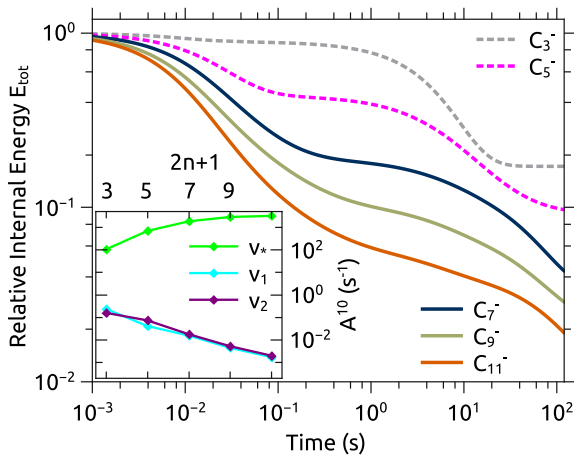
Fig. 6. Normalized total vibrational energy, E_{tot}, from master equation simulations, for the ensemble of stored ions as a function of time since formation for C_{2n+1}^- ($n = 3-5$, solid lines) as well as smaller odd-numbered clusters previously studied by Bull et al. [28] (dashed lines). Inset: Einstein coefficients for the brightest IR-active mode ν_* and low-energy modes ν_1 and ν_2 of C_{2n+1}^- clusters.

The time dependence of the photo-action yields in Figure 5 is consistent with infrared cooling according to SHC modelling (see Sect. 2.2). In Figure 6, we show results from master equation simulations of the total vibrational energy for the ensemble of stored ions $E_{tot}(t)$ as a function of time t after anion formation (normalized so that $E_{tot}(t = 0) = 1$). Note that the simulated curves do not account for the (small) fraction of the initial ion population that decays by thermionic emission because the initial energy distribution is not known and thus the fraction cannot be quantified. Compared with SHC modelling for C_3^- and C_5^- from the previous study of Bull et al. [28], the internal energy of the larger cluster anions considered in this work were found to decrease more rapidly during the first ~100 ms. Unfortunately, this initial rapid decay of E_{tot} is not well sampled by our 2D action spectroscopy method due to the 10 Hz repetition rate of the probe laser. However, after the initial decay, it is clear that the ultraslow dynamics within our measurement window (10^{-1} to 10^2 s) are significantly slower for cluster anions larger than C_5^-.

The SHC simulations in Figure 6 suggest that $E_{tot}(t)$ decreases rapidly between 0.1 s and 1 s. This stage of cooling is consistent with fitted $\tau_1 \approx 0.5$ s parameter from the photo-action data in Figure 5, which is attributed to lowering of internal energy to a point where the photoexcitation bands narrow and associated cross-sections increase. The SHC simulations (Fig. 6) then predict a slowing of energy liberation towards a plateau, e.g. 1 s–100 s (note the logarithmic scale), which is consistent with the second stage of cooling observed the experiment ($\tau_2 > 100$ s) compounded by the beam storage lifetime.

The increased rate of cooling at short storage times for C_7^-, C_9^-, and C_{11}^- compared with C_3^- and C_5^- from our earlier study is partly due to increasing infrared activity of the brightest modes $\nu_* = \nu_{13}$, ν_{18}, and ν_{21} for

$2n + 1 = 7$, 9, and 11, respectively (see Appendix A). The Einstein coefficients for these brightest modes, which completely dominate the cooling on short times, are plotted in the inset of Figure 6. Furthermore, due to increasing heat capacities with molecular size, larger clusters have a higher internal energy E_{tot} for a given initial temperature and are more likely to be formed with multiple quanta of ν_*. These modes are thus able to radiate a greater fraction of E_{tot} before ions are cooled to energies below $h\nu_*$. The slower cooling at longer storage times for the present target anions is a consequence of the decreasing activity of the two lowest frequency modes ν_1 and ν_2, also shown in the inset of Figure 6. These modes are responsible for the time-dependent hot-band contributions to the 2D action spectra in the previous study of C_n^- ($n = 3-5$) [28]; their reduced infrared activity leads to slower cooling for internal energies below $h\nu_*$.

As a final comment, improved quantification of the ultraslow cooling dynamics for C_7^-, C_9^- and C_{11}^- might be achieved with a narrow-linewidth laser, allowing for selective probing of detaching vibrational transitions. Improved characterization of the dynamics occurring on the sub-second timescale could be achieved through the use of a probe laser with a significantly higher repetition rate, e.g. 1 kHz.

4 Conclusions

We have probed the spontaneous slow and ultraslow relaxation dynamics of carbon cluster anions C_{2n+1} ($n = 3-5$) using two complementary strategies. First, we characterized spontaneous neutralization of the source-heated ions over the initial few milliseconds after injection into a cryogenic ion storage ring. The neutralization decay curves were well-reproduced by a statistical model combining thermionic emission and infrared radiative cooling. Second, we used two-dimensional (2D) near-threshold photodetachment action spectroscopy to probe the ultraslow cooling processes occurring up to 90 s after ion injection. Although the results indicated that ultraslow infrared cooling was considerably slower than for smaller carbon cluster anions [28] and hot bands were not evident, we were able to observe a time-dependence in the total neutralization yield for C_9^- and C_{11}^-. This time dependence was attributed to vibrational relaxation and associated increase of photo-excitation cross-sections, and was qualitatively described by a simple harmonic cascade model of radiative cooling via vibrational infrared emission.

The present experiments suggest that resonant excitation of electronic transitions, followed by internal conversion and thermionic emission (or dissociation), can lead to destruction of the anion. However, the first part of this process – internal conversion from an above-threshold resonance (or dipole-bound state) – is an established mechanism for anion formation in e.g. PAH-like molecules [5,52–54]. The key requirement to form a stable anion in space (if we assume that dissociation barriers are substantially higher than Φ) is $k_{IR}(E_r) > k_e(E_r)$, where k_{IR} is the rate coefficient for infrared emission, k_e is the rate coefficient

for thermionic emission, and E_r is the energy of the resonance. Values of k_e depend strongly upon electronic properties of the molecule, namely Φ and the electron capture cross section – see equation (2). In contrast, values of k_{IR} are sensitive to the vibrational properties and crucially the infrared activity (Eq. (1)). An "ideal" interstellar anion would have efficient internal conversion dynamics from excited electronic states to the ground electronic state, a high value of Φ (e.g. 3–4 eV), and be an efficient IR emitter. These properties may provide larger anions with many electronic states some resilience towards UV photodestruction (i.e., radiation up to a few eV above Φ), since photo-excitation cross-sections for conjugated molecules like PAHs are usually much larger than direct photodetachment cross-sections and the photo-excited anion could efficiently convert UV radiation into infrared radiation. Overall, it is highly desirable to have further measurements on thermionic emission and infrared radiative cooling properties of PAH and other carbonaceous anions (e.g. $C_{2n}H^-$ and $C_{2n}CN^-$ species) to draw more substantial conclusions about the interplay of these processes for the formation of stable interstellar anions. Understanding the slow and utlraslow relaxation dynamics in known interstellar anions allows prediction of lifecycles and abundances of other possible interstellar anions.

Author contribution statement

All authors contributed to planning, conducting and interpreting experiments. All authors discussed the manuscript.

Appendix A: Vibrational frequencies

Calculated harmonic vibrational frequencies ν_s scaled by factor 0.985 [28] and Einstein coefficients A_s^{10} (vibrational intensities) for C_{2n+1}^- ($n = 3-5$) and C_{2n+1} ($n = 3-5$) are given in Tables A.1–A.3.

Table A.1. Calculated vibrational frequencies and intensities for C_7^- and C_7.

| | C_7^- | | C_7 | |
Mode	ν (cm^{-1})	A^{10} (a.u.)	ν (cm^{-1})	A^{10} (a.u.)
ν_1	76.4	21.5	68.5	9.3
ν_2	84.6	20.0	68.5	9.3
ν_3	184.5	0.0	156.1	0.0
ν_4	189.0	0.0	156.1	0.0
ν_5	267.1	7.1	225.6	4.7
ν_6	350.1	1.8	225.6	4.7
ν_7	416.0	0.0	519.0	0.0
ν_8	421.7	0.0	519.0	0.0
ν_9	529.4	0.0	564.6	10.9
ν_{10}	571.1	0.0	564.6	10.9
ν_{11}	583.5	10.0	585.5	0.0
ν_{12}	1074.7	39.5	1113.8	5.1
ν_{13}	1593.8	5809.4	1611.4	0.0
ν_{14}	1617.7	0.0	1992.7	2196.6
ν_{15}	1967.4	194.2	2221.1	0.0
ν_{16}	2083.0	0.0	2232.6	8337.0

Table A.2. Calculated vibrational frequencies and intensities for C_9^- and C_9.

| | C_9^- | | C_9 | |
Mode	ν (cm^{-1})	A^{10} (a.u.)	ν (cm^{-1})	A^{10} (a.u.)
ν_1	46.9	16.3	43.6	6.8
ν_2	52.0	15.6	43.6	6.8
ν_3	120.2	0.0	109.1	0.0
ν_4	135.6	0.0	109.1	0.0
ν_5	208.4	11.9	183.0	8.1
ν_6	216.8	7.8	183.0	8.1
ν_7	267.1	0.0	236.9	0.0
ν_8	338.7	0.0	236.9	0.0
ν_9	373.5	0.1	461.0	0.0
ν_{10}	443.9	0.3	481.1	0.7
ν_{11}	451.8	0.0	481.1	0.7
ν_{12}	464.5	0.0	530.0	13.7
ν_{13}	491.5	0.3	530.0	13.7
ν_{14}	553.8	13.6	541.4	0.0
ν_{15}	558.9	0.0	541.4	0.0
ν_{16}	865.0	175.6	890.0	3.2
ν_{17}	1248.7	0.0	1289.1	0.0
ν_{18}	1359.8	12 436.5	1670.5	455.7
ν_{19}	1695.5	235.1	1979.6	0.0
ν_{20}	1969.6	0.0	2100.6	16 400.8
ν_{21}	2075.0	1540.9	2209.4	5035.3
ν_{22}	2149.8	0.0	2279.2	0.0

Table A.3. Calculated vibrational frequencies and intensities for C_{11}^- and C_{11}.

Mode	C_{11}^-		C_{11}	
	$\nu\,(\text{cm}^{-1})$	$A^{10}\,(\text{a.u.})$	$\nu\,(\text{cm}^{-1})$	$A^{10}\,(\text{a.u.})$
ν_1	32.3	13.2	31.4	5.4
ν_2	35.4	12.8	31.4	5.4
ν_3	82.9	0.0	77.7	0.0
ν_4	92.4	0.0	77.7	0.0
ν_5	152.9	11.0	140.5	7.6
ν_6	170.3	9.7	140.5	7.6
ν_7	223.3	0.0	201.3	0.0
ν_8	234.1	0.0	201.3	0.0
ν_9	267.8	3.6	244.2	2.5
ν_{10}	331.4	1.1	244.2	2.5
ν_{11}	373.0	0.0	379.4	0.0
ν_{12}	388.9	0.0	468.4	0.0
ν_{13}	437.7	0.0	468.4	0.0
ν_{14}	473.4	0.0	517.1	0.0
ν_{15}	481.2	0.0	517.1	0.0
ν_{16}	487.7	1.7	537.5	0.0
ν_{17}	531.9	0.0	537.5	0.0
ν_{18}	557.5	0.0	554.5	17.1
ν_{19}	573.7	17.1	554.5	17.1
ν_{20}	718.9	655.2	739.8	20.7
ν_{21}	1051.2	23 258.8	1078.8	0.0
ν_{22}	1053.5	0.0	1399.3	105.7
ν_{23}	1359.9	205.7	1709.8	0.0
ν_{24}	1725.8	0.0	1946.2	8672.7
ν_{25}	1970.8	271.3	2072.6	31 145.5
ν_{26}	2064.8	0.0	2114.3	0.0
ν_{27}	2155.5	4152.1	2247.7	4.5
ν_{28}	2156.0	0.0	2284.2	0.0

References

1. K. Hansen, *Statistical Physics of Nanoparticles in the Gas Phase* (Springer, 2013)
2. H. Handschuh, G. Ganteför, B. Kessler, P.S. Bechthold, W. Eberhardt, Phys. Rev. Lett. **74**, 1095 (1995)
3. R. Jones, G. Seifert, Phys. Rev. Lett. **79**, 443 (1997)
4. S. Petrie, D.K. Bohme, Mass Spectrom. Rev. **26**, 258 (2007)
5. T.J. Millar, C. Walsh, T.A. Field, Chem. Rev. **117**, 1765 (2017)
6. J. Cernicharo, M. Guélin, M. Agúndez, K. Kawaguchi, M. McCarthy, P. Thaddeus, Astron. Astrophys. **467**, L37 (2007)
7. M.C. McCarthy, C.A. Gottlieb, H. Gupta, P. Thaddeus, Astrophys. J. Lett. **652**, L141 (2006)
8. S. Brünken, H. Gupta, C.A. Gottlieb, M.C. McCarthy, P. Thaddeus, Astrophys. J. Lett. **664**, L43 (2007)
9. M. Agúndez, J. Cernicharo, M. Guélin, C. Kahane, E. Roueff, J. Kłos, F.J. Aoiz, F. Lique, N. Marcelino, J.R. Goicoechea, M.G. García, C.A. Gottlieb, M.C. McCarthy, P. Thaddeus, Astron. Astrophys. **517**, L2 (2010)
10. P. Thaddeus, C.A. Gottlieb, H. Gupta, S. Brünken, M.C. McCarthy, Astrophys. J. **677**, 1132 (2008)
11. J. Cernicharo, M. Guélin, M. Agúndez, M.C. McCarthy, P. Thaddeus, Astrophys. J. Lett. **688**, L83 (2008)
12. J.U. Andersen, C. Gottrup, K. Hansen, P. Hvelplund, M.O. Larsson, Eur. Phys. J. D **17**, 189 (2001)
13. J.U. Andersen, H. Cederquist, J.S. Forster, B.A. Huber, P. Hvelplund, J. Jensen, B. Liu, B. Manil, L. Maunoury, S. Brøndsted Nielsen, U.V. Pedersen, H.T. Schmidt, S. Tomita, H. Zettergren, Eur. Phys. J. D **25**, 139 (2003)
14. Y. Toker, O. Aviv, M. Eritt, M. Rappaport, O. Heber, D. Schwalm, D. Zajfman, Phys. Rev. A **76**, 053201 (2007)
15. O. Aviv, Y. Toker, D. Strasser, M. Rappaport, O. Heber, D. Schwalm, D. Zajfman, Phys. Rev. A **83**, 023201 (2011)
16. M.W. Froese, K. Blaum, F. Fellenberger, M. Grieser, M. Lange, F. Laux, S. Menk, D.A. Orlov, R. Repnow, T. Sieber, Y. Toker, R. von Hahn, A. Wolf, Phys. Rev. A **83**, 023202 (2011)
17. S. Martin, J. Bernard, R. Brédy, B. Concina, C. Joblin, M. Ji, C. Ortega, L. Chen, Phys. Rev. Lett. **110**, 063003 (2013)
18. M. Goto, A.E.K. Sundén, H. Shiromaru, J. Matsumoto, H. Tanuma, T. Azuma, K. Hansen, J. Chem. Phys. **139**, 054306 (2013)
19. S. Menk, S. Das, K. Blaum, M.W. Froese, M. Lange, M. Mukherjee, R. Repnow, D. Schwalm, R. von Hahn, A. Wolf, Phys. Rev. A **89**, 022502 (2014)
20. K. Najafian, M.S. Pettersson, B. Dynefors, H. Shiromaru, J. Matsumoto, H. Tanuma, T. Furukawa, T. Azuma, K. Hansen, J. Chem. Phys. **140**, 104311 (2014)
21. M. Ji, J. Bernard, L. Chen, R. Brédy, C. Ortéga, C. Joblin, A. Cassimi, S. Martin, J. Chem. Phys. **146**, 044301 (2017)
22. G. Ito, T. Furukawa, H. Tanuma, J. Matsumoto, H. Shiromaru, T. Majima, M. Goto, T. Azuma, K. Hansen, Phys. Rev. Lett. **112**, 183001 (2014)
23. V. Chandrasekaran, B. Kafle, A. Prabhakaran, O. Heber, M. Rappaport, H. Rubinstein, D. Schwalm, Y. Toker, D. Zajfman, J. Phys. Chem. Lett. **5**, 4078 (2014)
24. C. Breitenfeldt, K. Blaum, M.W. Froese, S. George, G. Guzmán-Ramírez, M. Lange, S. Menk, L. Schweikhard, A. Wolf, Phys. Rev. A **94**, 033407 (2016)
25. K. Hansen, M.H. Stockett, M. Kaminska, R.F. Nascimento, E.K. Anderson, M. Gatchell, K.C. Chartkunchand, G. Eklund, H. Zettergren, H.T. Schmidt, H. Cederquist, Phys. Rev. A **95**, 022511 (2017)
26. E.K. Anderson, M. Kamińska, K.C. Chartkunchand, G. Eklund, M. Gatchell, K. Hansen, H. Zettergren, H. Cederquist, H.T. Schmidt, Phys. Rev. A **98**, 022705 (2018)
27. C. Breitenfeldt, K. Blaum, S. George, J. Göck, G. Guzmán-Ramírez, J. Karthein, T. Kolling, M. Lange, S. Menk, C. Meyer, J. Mohrbach, G. Niedner-Schatteburg, D. Schwalm, L. Schweikhard, A. Wolf, Phys. Rev. Lett. **120**, 253001 (2018)
28. J.N. Bull, M.S. Scholz, E. Carrascosa, M.K. Kristiansson, G. Eklund, N. Punnakayathil, N. de Ruette, H. Zettergren, H.T. Schmidt, H. Cederquist, M.H. Stockett, J. Chem. Phys. **151**, 114304 (2019)
29. M.H. Stockett, M. Björkhage, H. Cederquist, H. Schmidt, H. Zettergren, Faraday Discuss. **217**, 126 (2019)
30. R.D. Thomas, H.T. Schmidt, G. Andler, M. Björkhage, M. Blom, L. Brännholm, E. Bäckström, H. Danared, S. Das, N. Haag, P. Halldén, F. Hellberg, A.I.S. Holm, H.A.B. Johansson, A. Källberg, G. Källersjö, M. Larsson, S. Leontein, L. Liljeby, P. Löfgren, B. Malm, S. Mannervik, M. Masuda, D. Misra, A. Orbán, A. Paál, P. Reinhed, K.G. Rensfelt, S. Rosén, K. Schmidt, F. Seitz,

A. Simonsson, J. Weimer, H. Zettergren, H. Cederquist, Rev. Sci. Instrum. **82**, 065112 (2011)

31. H.T. Schmidt, R.D. Thomas, M. Gatchell, S. Rosén, P. Reinhed, P. Löfgren, L. Brännholm, M. Blom, M. Björkhage, E. Bäckström, J.D. Alexander, S. Leontein, D. Hanstorp, H. Zettergren, L. Liljeby, A. Källberg, A. Simonsson, F. Hellberg, S. Mannervik, M. Larsson, W.D. Geppert, K.G. Rensfelt, H. Danared, A. Paál, M. Masuda, P. Halldén, G. Andler, M.H. Stockett, T. Chen, G. Källersjö, J. Weimer, K. Hansen, H. Hartman, H. Cederquist, Rev. Sci. Instrum. **84**, 055115 (2013)

32. E. Bäckström, D. Hanstorp, O.M. Hole, M. Kaminska, R.F. Nascimento, M. Blom, M. Björkhage, A. Källberg, P. Löfgren, P. Reinhed, S. Rosén, A. Simonsson, R.D. Thomas, S. Mannervik, H.T. Schmidt, H. Cederquist, Phys. Rev. Lett. **114**, 143003 (2015)

33. H.T. Schmidt, G. Eklund, K.C. Chartkunchand, E.K. Anderson, M. Kamińska, N. de Ruette, R.D. Thomas, M.K. Kristiansson, M. Gatchell, P. Reinhed, S. Rosén, A. Simonsson, A. Källberg, P. Löfgren, S. Mannervik, H. Zettergren, H. Cederquist, Phys. Rev. Lett. **119**, 073001 (2017)

34. S. Rosén, H.T. Schmidt, P. Reinhed, D. Fischer, R.D. Thomas, H. Cederquist, L. Liljeby, L. Bagge, S. Leontein, M. Blom, Rev. Sci. Instrum. **78**, 113301 (2007)

35. E.K. Anderson, Desiree: instrumentation developments and hot metal cluster decays, Ph.D. thesis, Department of Physics, Stockholm University, 2019

36. J.D. Chai, M. Head-Gordon, Phys. Chem. Chem. Phys. **10**, 6615 (2008)

37. T.H. Dunning Jr., J. Chem. Phys. **90**, 1007 (1989)

38. M.J. Frisch, G.W. Trucks, H.B. Schlegel, G.E. Scuseria, M.A. Robb, J.R. Cheeseman, G. Scalmani, V. Barone, B. Mennucci, G.A. Petersson, H. Nakatsuji, M. Caricato, X. Li, H.P. Hratchian, A.F. Izmaylov, J. Bloino, G. Zheng, J.L. Sonnenberg, M. Hada, M. Ehara, K. Toyota, R. Fukuda, J. Hasegawa, M. Ishida, T. Nakajima, Y. Honda, O. Kitao, H. Nakai, T. Vreven, J.A. Montgomery, Jr., J.E. Peralta, F. Ogliaro, M. Bearpark, J.J. Heyd, E. Brothers, K.N. Kudin, V.N. Staroverov, R. Kobayashi, J. Normand, K. Raghavachari, A. Rendell, J.C. Burant, S.S. Iyengar, J. Tomasi, M. Cossi, N. Rega, J.M. Millam, M. Klene, J.E. Knox, J.B. Cross, V. Bakken, C. Adamo, J. Jaramillo, R. Gomperts, R.E. Stratmann, O. Yazyev, A.J. Austin, R. Cammi, C. Pomelli, J.W. Ochterski, R.L. Martin, K. Morokuma, V.G. Zakrzewski, G.A. Voth, P. Salvador, J.J. Dannenberg, S. Dapprich, A.D. Daniels, O. Farkas, J.B. Foresman, J.V. Ortiz, J. Cioslowski, D.J. Fox, *Gaussian 16 Revision B.01* (Gaussian Inc., Wallingford, CT, 2016)

39. N. Kono, T. Furukawa, H. Tanuma, J. Matsumoto, H. Shiromaru, T. Azuma, K. Najafian, M.S. Pettersson, B. Dynefors, K. Hansen, Phys. Chem. Chem. Phys. **17**, 24732 (2015)

40. Y. Ebara, T. Furukawa, J. Matsumoto, H. Tanuma, T. Azuma, H. Shiromaru, K. Hansen, Phys. Rev. Lett. **117**, 133004 (2016)

41. N. Kono, R. Suzuki, T. Furukawa, J. Matsumoto, H. Tanuma, H. Shiromaru, T. Azuma, K. Hansen, Phys. Rev. A **98**, 063434 (2018)

42. J.U. Andersen, E. Bonderup, K. Hansen, J. Phys. B **35**, R1 (2002)

43. M.C. Babin, J.A. DeVine, M.L. Weichman, D.M. Neumark, J. Chem. Phys. **149**, 174306 (2018)

44. D.W. Arnold, S.E. Bradforth, T.N. Kitsopoulos, D.M. Neumark, J. Phys. Chem. **95**, 8753 (1991)

45. W.D. Price, P.D. Schnier, E.R. Williams, J. Phys. Chem. B **101**, 664 (1997)

46. M.J. Deluca, M.A. Johnson, Chem. Phys. Lett. **152**, 67 (1988)

47. Y. Tai, J. Murakami, Y. Maruyama, W. Yamaguchi, T. Mizota, K. Igarashi, S. Tanemura, J. Phys. Chem. B **103**, 5500 (1999)

48. F. Lépine, A.R. Allouche, B. Baguenard, C. Bordas, M. Aubert-Frécon, J. Phys. Chem. A **106**, 7177 (2002)

49. K. Hansen, J.U. Andersen, P. Hvelplund, S.P. Møller, U.V. Pedersen, V.V. Petrunin, Phys. Rev. Lett. **87**, 123401 (2001)

50. D. Forney, M. Grutter, P. Freivogel, J.P. Maier, J. Phys. Chem. A **101**, 5292 (1997)

51. E.P. Wigner, Phys. Rev. **73**, 1002 (1984)

52. P.J. Sarre, Mon. Not. R. Astron. Soc. **313**, L14 (2002)

53. J.N. Bull, C.W. West, J.R.R. Verlet, Chem. Sci. **6**, 1578 (2015)

54. J.N. Bull, C.W. West, J.R.R. Verlet, Phys. Chem. Chem. Phys. **17**, 32464 (2015)